Proceedings World Geothermal Congress 2020+1
Reykjavik, Iceland, April - October 2021

Applications of Hyperspectral Imaging to Geothermal Drill Core and Cuttings: Case Studies from Nevada, Western USA

Kurt O. Kraal, Bridget Ayling and Wendy Calvin

Great Basin Centre for Geothermal Energy, University of Nevada, Reno. 1664 N Virginia St, Reno, NV 89557, USA

kokraal@nevada.unr.edu, bayling@unr.edu, wcalvin@unr.edu

Keywords: Hyperspectral, infrared spectroscopy, hydrothermal alteration, Nevada, great basin, drill core, Fallon FORGE, Tungsten Mountain, EGS, SWIR

ABSTRACT

Infrared spectroscopy is effective for analysing geologic materials because most rock-forming minerals have absorption features in the short-wave infrared (1000-2500 nm, SWIR) and long-wave infrared (2.5-25 μm, LWIR). Applied to drill core or cuttings samples, infrared spectroscopy is useful for characterising the lithologies and minerals encountered in geothermal wells. The type and distribution of hydrothermal alteration mineralogy within a well provides information about past temperatures, field hydrology, and rock physical properties. In this study, we apply advances in hyperspectral imaging technology to create high-resolution mineral maps of geothermal drill core and cuttings samples to characterise reservoir lithologies and alteration assemblages. The primary instrument used in this study is equipped with VNIR-SWIR (500-2500 nm) and LWIR (7.6-11.9 μm) spectral cameras that have a pixel size of 1.2 mm, as well as an RGB camera, to create a high resolution (0.12 mm pixel size) image of the same drill core or cuttings sample. Hyperspectral imaging allows for rapid analyses with minimal sample preparation and allows for the evaluation of the spatial relationships of alteration minerals within samples, with depth, and between wells at higher spatial resolutions than typically applied to geothermal systems. We investigate two field sites from Nevada, western USA: the Tungsten Mountain geothermal field, operated by Ormat Nevada, Inc., and the Fallon FORGE Engineered Geothermal System (EGS) site. These two locations represent contrasting geothermal endmembers: an active hydrothermal system (Tungsten Mountain, currently with 37 MWe installed capacity) and low permeability, conductive geothermal system (the Fallon FORGE EGS site). At both locations, we analyse samples from several wells in the 300 to 2800 m depth range and use infrared spectroscopy to characterise the distribution of minerals at various scales. Comparison of these new hyperspectral data with existing datasets (e.g. structural, stratigraphic, geophysical, mineralogical, hydrologic, temperature) can reveal new insights on the relationship of hydrothermal alteration to reservoir properties, with implications for geothermal reservoir characterisation, and hydrothermal alteration history.

1. INTRODUCTION

The Great Basin geothermal province of the western United States is home to more than 400 known geothermal systems with ~25 plants and a total installed capacity of 720 MWe in Nevada as of 2017 (Ayling, 2018). The majority of the geothermal systems in the Great Basin are amagmatic systems, meaning they derive their heat from high geothermal gradients in the crust, rather than from shallow-mid crustal magma bodies (Henley and Brown, 1985; Faulds et al., 2004). It has been suggested that the potential power generation in the region is much greater: as much as 30,000 MW (Williams et al., 2007). To reach this potential, there are significant challenges in the exploration and development of Great Basin geothermal systems.

The type and distribution of hydrothermal alteration minerals within geothermal systems provide information regarding past temperatures, fluid flow pathways, fluid chemistry and rock properties that are important for exploration and reservoir characterisation (Henley and Ellis, 1983; Reyes, 1990). Thermal structures of geothermal fields are often reflected in a zonation of alteration minerals, typically with a low temperature smectite zone near the surface, an interlayered illite-smectite zone at moderate temperatures, and an illite or illite-chlorite zone in the hotter parts of the system (Browne, 1978; Henley and Ellis, 1983; Reyes, 1990). In addition, certain minerals are associated with permeable zones, impermeable zones, zones of steam-heated acidic waters, or cold-water influx (Reyes, 1990). The hydrothermal alteration also affects rock physical properties such as resistivity, permeability, porosity, density, strength and ultrasonic pulse velocities (Frolova et al., 2014; Wyering et al., 2014). In addition to applications in conventional convective hydrothermal systems, alteration mineralogy studies are important for EGS (Enhanced/Engineered Geothermal Systems) because EGS sites require extensive characterisation in terms of thermal regime and reservoir rock properties (e.g. Dezayes, 2010).

Infrared reflectance spectroscopy is an effective tool to rapidly collect mineralogical data from geothermal drill core or cuttings samples, including clay minerals that are difficult to distinguish in hand sample or by petrography (Thompson, 1999; Calvin and Pace, 2016). Also, it does not require the lengthy sample preparation required for X-Ray Diffraction (XRD) analysis. This method is effective because most rock-forming minerals have diagnostic absorption features in either the Visible-Near Infrared to Short-Wave Infrared (VNIR-SWIR, 400-2500 nm) or the Long Wave Infrared (LWIR, 8-12 μm) (Clark, 1999). This method is regularly applied to exploration for hydrothermal ore deposits (Thompson, 1999; Herrmann et al., 2001; Mauger et al., 2007). Applications to active geothermal systems include remote sensing (van der Meer et al., 2014), a pilot study by Calvin and Pace (2016) applied to drill core and cuttings from geothermal systems using a portable SWIR spectroradiometer, and other studies in New Zealand using SWIR (Yang et al., 2000, 2001; Mauriohooho et al., 2014; Simpson and Rae, 2018; Glaas et al., 2019). These analyses can provide similar information as XRD, such as clay mineral type, but can be performed at much higher spatial resolution due to faster analyses, low sample preparation requirements, and lower cost. When used along with XRD of selected intervals, infrared spectroscopy can fill in the gaps between measurements, and better delineate boundaries between lithologies and alteration types, as well as a chance to identify features previously missed by wider spaced XRD sampling.

The aims of this study are to apply for advances in high-spatial-resolution imaging spectroscopy to investigate the distribution of hydrothermal alteration minerals within geothermal drill core and cuttings samples using case studies from the Great Basin. We intend to use the data as: 1) a geothermometer of past hydrothermal conditions by investigating the location of the smectite-illite transition; 2) a guide to locations of past fluid flow and fluid type based on analysis of hydrothermal alteration style, potentially giving insight into multiple phases of hydrothermal alteration; and 3) a method to characterize reservoir rocks in terms of mineralogical variability.

2. BACKGROUND

2.1 Great Basin Geology

The Great Basin of the western United States has a complex geologic history, which manifests as a wide variety of lithologies encountered in modern-day geothermal fields. From the Neoproterozoic to the middle Palaeozoic, the area known today as the Great Basin was a passive margin environment where sedimentary rocks were deposited (Burke and Silberling, 1973; Wyld, 2002; Dickinson, 2004; Decelles, 2004). These lithologies underwent deformation through tectonism during orogenies such as the Nevadan, and Sevier (Dickinson, 2006). In the Jurassic-Cretaceous, the sedimentary and volcanic rocks were intruded by numerous granitic-granodioritic plutons linked to subduction magmatism (Van Buer et al., 2009). These lithologies make up the basement rocks hosting the geothermal systems in the Great Basin today. Beginning in Eocene-Oligocene, volcanic rocks and ash-flow tuffs from a series of volcanic events eventually covered much of western Nevada (Faulds et al., 2005; Henry et al., 2012; Henry and John, 2013;John et al., 2014), however most of the volcanism in the region ceased around 3 Ma (Dickinson, 2006). Many of the Great Basin's mineral deposits and associated fossil hydrothermal systems are related to the successive stages of past volcanism. The modern Basin and Range topography was the product of regional extension that began in the late Miocene and reached north-western Nevada about 12 Ma (Faulds and Henry, 2005). Basin and Range extension is characterised by N-S-trending, E-W extending normal fault systems. This process also elevated the crustal heat flow by thinning the crust, providing the heat source for geothermal systems (Faulds et al., 2004).

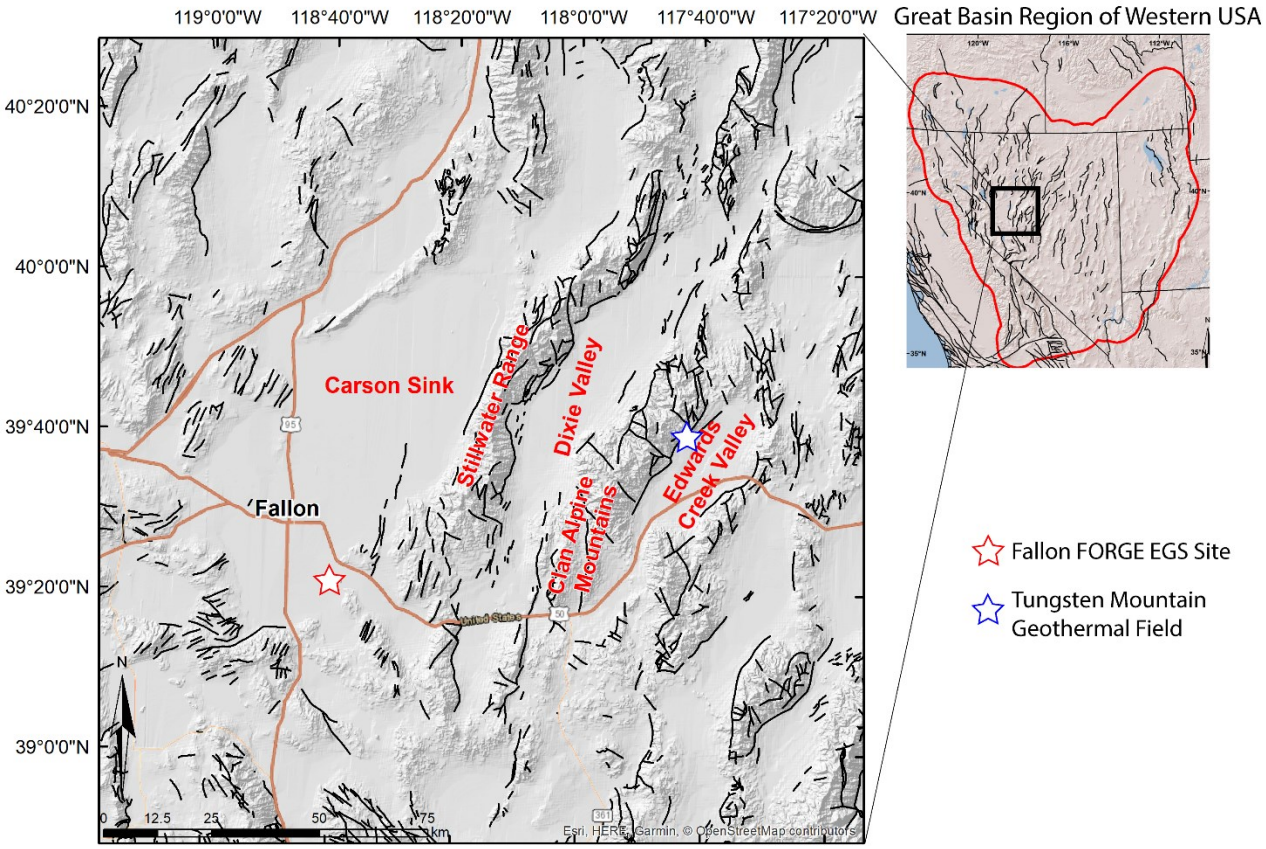

Figure 1: Location of field areas addressed in this study, as well as regional features referenced herein.

2.2 Fallon FORGE EGS Site

The Fallon FORGE EGS site is located in Churchill County, Nevada, and was previously evaluated as a test site for the Frontier Observatory for Research in Geothermal Energy (FORGE) initiative managed by the US Department of Energy (Figure 1). Although not chosen to host the FORGE laboratory, a detailed geoscientific characterisation of the Fallon FORGE site was conducted by the Fallon FORGE team during phase 1 and phase 2 including the drilling of a 2,460 m (8,104 ft) well in February-March 2018 (Faulds et al., 2018; Siler et al., 2018). Structurally, the site is located within a west-tilted half-graben that is cut by widely spaced normal faults (Siler et al., 2018). The lithologies encountered in wells at the site include: 1) Quaternary-Tertiary basin-fill sediments, 2) Miocene mafic volcanics, primarily basaltic andesite, with some lithic tuff, andesite, rhyodacite, and volcanic breccia, 3) quartz monzonite intrusions of unknown age, 4) pre-Miocene altered-basalt and basaltic andesite, 5) possibly Mesozoic quartzite, with lesser marble, meta-mudstone, and altered-volcanics, 6) pre-Miocene altered-rhyolite tuff and flows with lesser basaltic andesite

(Blankenship, 2018, Figure 2). The primary formation proposed for EGS stimulation is altered-rhyolite. Four >2,100 m depth wells terminate in the pre-Miocene lithologies within the FORGE site record maximum bottom whole temperatures of 194-214 °C (Blankenship, 2016; Siler et al., 2016). Temperature profiles of these wells indicate primarily conductive gradients, with discrete zones of possible wellbore crossflow. Data and analysis from the most recently drilled well, 21-31, was presented in Kraal et al., 2021.

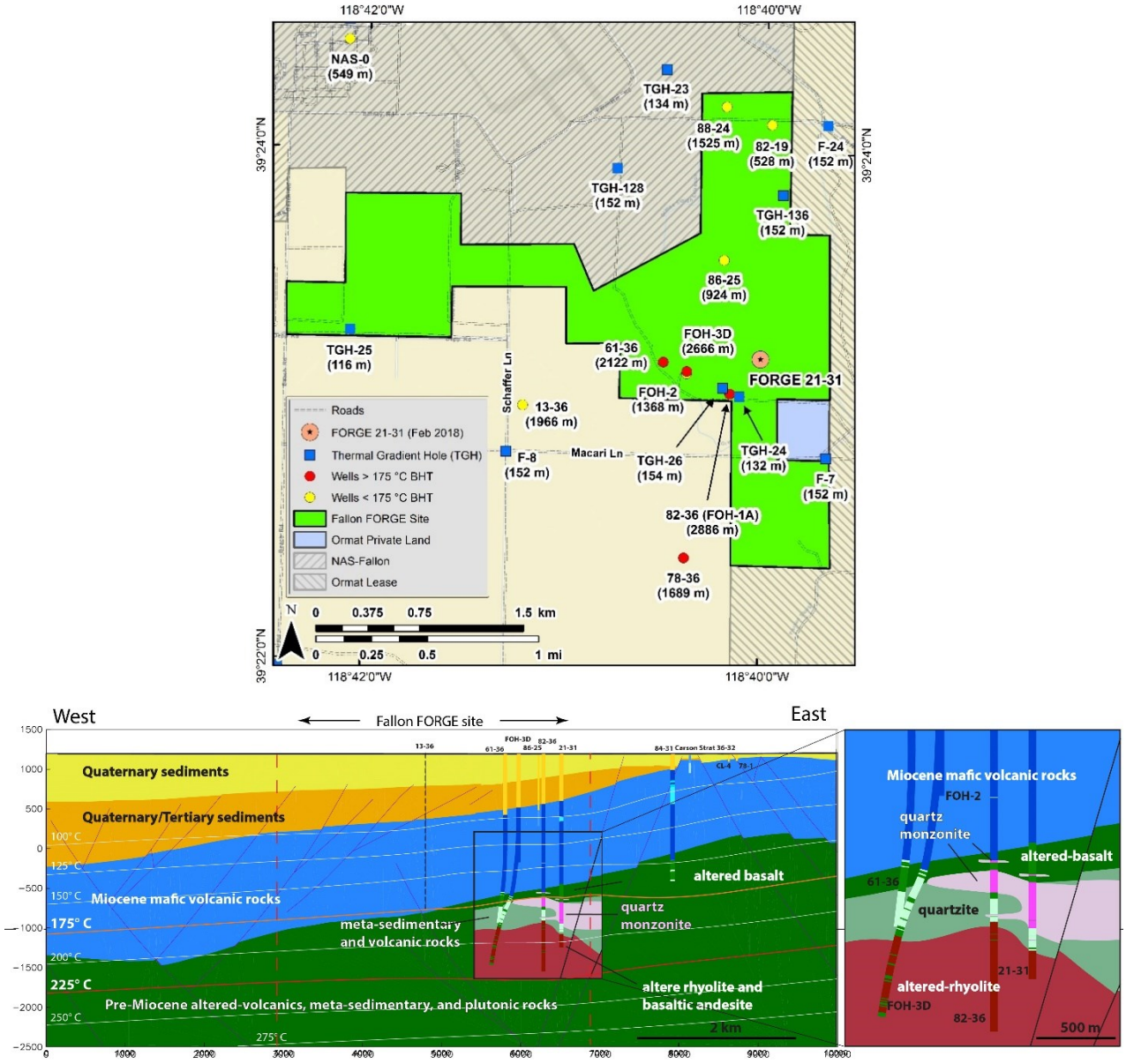

Figure 2: Fallon FORGE EGS site well locations map, and cross-section from the geologic model, and model insert (adapted from Siler et al., 2019). Wells investigated in this study include well 21-31, 82-36, and FOH-3D. Ages of pre-Miocene lithologic units currently under investigation.

2.3 Tungsten Mountain Geothermal Field

The Tungsten Mountain Geothermal Field is located in Edwards Creek Valley, on the eastern flank of the Clan Alpine Mountains of Churchill County, Nevada (Figure 1). The Clan Alpine Mountains trend northward, and are fault-bounded (Willden and Speed, 1974). The mountains expose Mesozoic rocks that include deformed Triassic siltstone, Upper Triassic carbonate rocks, and moderately dipping Triassic and Jurassic volcanic sedimentary rocks (Willden and Speed, 1974). The range hosts many exposed intrusive igneous rocks including numerous small Cretaceous granodiorites. The Clan Alpines contain thick sequences of Tertiary volcanic rocks that include both rhyolites, andesites, and basalts (Willden and Speed, 1974). Edwards Creek valley is separated from the eastern margin of the Clan Alpine Mountains by the Clan Alpine fault zone. Structurally, Edwards Creek valley is west-dipping half-graben, with more faulting observed on the west flank than the east. Like many Nevada basins, Edwards Creek valley is covered in Quaternary alluvial fan surfaces and lake sediments (Machette et al., 2015).

The Tungsten Mountain geothermal field is located adjacent to Tungsten Mountain near Stone Canyon, at a normal fault step-over containing numerous overlapping fault intersections (Figure 3; Delwiche, 2018;). The primary lithology contains about 150-1000 m

(500-3200 ft) of Quaternary-Tertiary fill upon Tertiary ash-flow tuffs and andesite flows that cap Triassic metasedimentary rocks, with some granodiorite and tonalite intrusions (Delwiche et al., 2018). The primary geothermal fluid flow pathways appear to be in damage zones of faults, particularly within northeast striking faults in the Triassic meta-sedimentary rock unit, but also at intersections between northeast striking and west-northwest striking faults in some locations (Delwiche et al., 2018). Since November 2017, the Tungsten Mountain geothermal field has produced 26 MWe net power production, with a resource temperature of ~143 °C (290 °F) (Ayling, 2018; Delwiche et al., 2018).

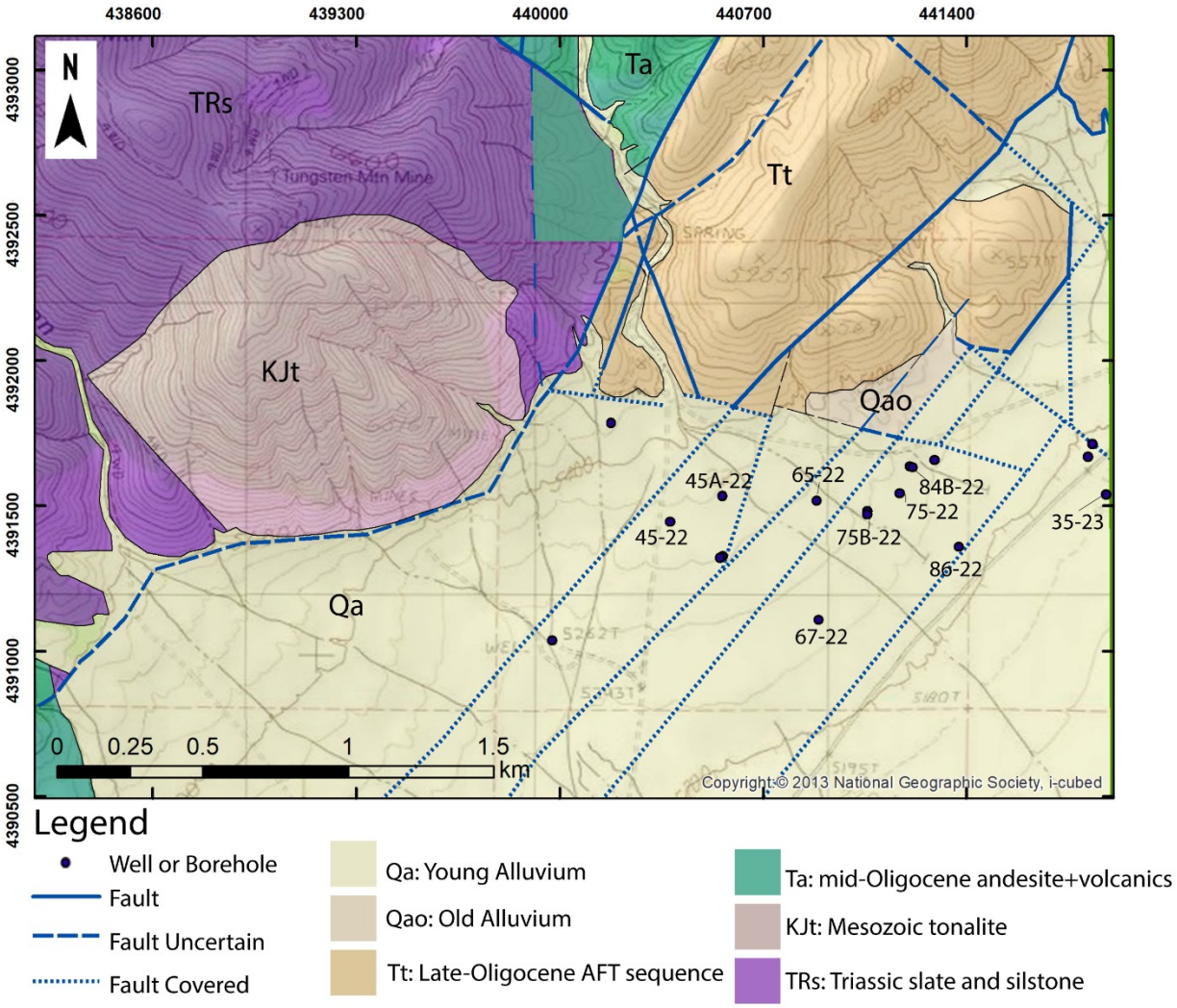

Figure 3: Map of Tungsten Mountain geothermal field (operated by Ormat Nevada, Inc.). Well locations investigated in this study are also shown. Adapted from Delwiche et al., 2018.

2.4 Infrared Spectroscopy

With infrared reflectance spectroscopy, minerals are identified based on the shape and location of absorption features in the sample's spectrum. A spectrum is a representation of the reflectance of light for each wavelength in the range analysed. Absorption features in the infrared range are caused by either vibrational processes, due to bonds in the crystal lattice, or electronic processes, due to unfilled d orbitals (Clark, 1999). Molecules that show absorption features in the SWIR are OH, C-O, cation-OH (Clark, 1999). The LWIR range is sensitive to the Si-O, P-O, and C-O bonds (Salisbury et al., 1991). VNIR is useful for distinguishing Fe bearing oxide minerals. SWIR is especially effective for hydrated silicate minerals, such as phyllosilicates - such as clays and chlorites -, amphiboles, in addition to carbonates. LWIR is useful for silicates, carbonates, and phosphates, including non-hydrated minerals that do not have absorption features in the SWIR. Sample spectra are compared with spectral reference libraries, such as the U.S. Geological Survey, or the John Hopkins for mineral identification (Clark et al., 1990; Salisbury et al., 1991). In addition to mineral type, absorption bands are sensitive to crystal structure and subtle changes in chemistry (Clark, 1999).

Hyperspectral core imaging/scanning is a new development for analysing the distribution of minerals within a core or cuttings sample. Hyperspectral image datasets can be continuous across many meters of the core at high spatial resolution (1 mm pixel size or less), which can give spatial context to observed spectra. There are many varieties of core imaging/scanning instruments, which range from devices designed to collect data along lines following the centre of the core, and those that image/scan entire core boxes to create a 2-dimensional image which can be processed similar to remote sensing data. Core imaging using SWIR spectroscopy has been used to map alteration in core from ore deposits (Huntington et al., 2006; Tappert et al., 2011; Kokaly et al., 2017; Zhou et al., 2017), and

hydrocarbon exploration (Ayling et al., 2016; Mehmani et al., 2017). However, there are relatively few published studies of hyperspectral core imaging for geothermal applications (e.g., Kraal et al., 2018; Waweru, 2019; Kraal et al., 2021)

3. METHODS

3.1 Hyperspectral Instruments

The TerraCore hyperspectral imaging instrument used in this study operates via stationary line-scanning cameras, where the core box is placed on a table that is passed underneath the cameras at a controlled rate. This method allows for imaging the entire core box, with an average image collection speed of approximately 90 seconds. During each scan, a white and dark reference is collected for image calibration. This instrument utilises 411 bands covering the VNIR-SWIR (463 nm – 2476 nm) and an additional camera covering the LWIR (8-12 μm) range with sampling approximately every 5 nm. The FENIX VNIR-SWIR and OWL LWIR spectral cameras have a pixel size of 1.2 mm. In addition to a hyperspectral image, an RGB camera creates a high resolution (0.12 mm pixel size) image of the same drill core simultaneously.

Additional hyperspectral "spot" measurements were performed using an ASD FieldSpec Pro portable spectroradiometer that measures in the VNIR/SWIR range to collect spectra from core and cuttings. The data collection targeted both zones of alteration and unaltered rock. Spectral data at each "spot" represent mixtures of minerals located within the instrument's 20 mm diameter field of view. The data collection calibrates the observation relative to a white halon plate so that the resulting measurement is one of calibrated reflectance that can be directly compared to library spectra for mineral identification.

3.2 Spectral Data Processing

Spectral data derived from the hyperspectral images are converted to reflectance, and the extraneous material such as the core box is masked to avoid mixed spectra from interfering with mineral identification. Spectra from the images are then separated into composite endmembers using TerraCore's proprietary software. Each spectral endmember represents a unique spectral composite shape in a given image that may be composed of a single mineral or a mineral mixture. Endmembers are chosen based on a combination of spectral variability and spatial occurrence. Images created include mineral maps demonstrating mineralogical variance, and feature extractions of numerical data such as spectral scalars. For hyperspectral spot measurements, spectra are interpreted individually and given an assigned mineral or mineral mixture based on comparison with library spectra (Clark, 1990). Spectral interpretations from each sample are plotted with depth to observe changes in dominant mineralogy and spectral scalars.

Spectral scalars are numerical data derived from the spectra, such as the depth or location of an absorption feature. Scalars provide additional information about mineral chemistry and abundance (Clark, 1999). These include illite/mica composition (related to the location of the 2200 nm Al-OH absorption feature, chlorite composition (related to the location of the 2250 nm feature), and "illite maturity", related to the relative feature depths of the 1900 nm H_2O and 2200 nm Al-OH nm features, a proxy related to the relative amounts of smectite versus illite minerals (Pontual et al., 1997; Yang et al., 2011; Simpson and Rae, 2018). In this study, illite maturity was calculated by dividing the hull corrected reflectance minimum of the 1900 nm absorption feature, by the hull corrected reflectance minimum of the 2200 nm feature. Al-OH wavelength was calculated as the wavelength between 2180 and 2232 nm with the lowest hull corrected reflectance, excluding measurements where the lowest reflectance was at the wavelength endpoints.

One technique for assessing changes in SWIR or LWIR responsive mineralogy with depth was developed using the hyperspectral imaging of cuttings samples. For alternating cuttings samples from well 21-31 from the Fallon FORGE site, cuttings were spread out on a black background and completely imaged. This method allowed for the calculation of sample area displaying each endmember spectra. Using this data, we plotted dominant mineral sample area with depth, which allows for a useful figure to visualise changes in spectrally dominant mineralogy with depth, as well as average spectral scalar values for each sample (Figure 11).

3.3 Sample Types and Analyses Performed

Samples used in this study include drill core, drill cuttings, and sidewall cores. From the Fallon site, hyperspectral images were collected from cuttings samples derived from three wells (21-31, FOH-3D, 82-36), and 54 sidewall cores from well 21-31. From the Tungsten Mountain site, hyperspectral images were collected from 130 core boxes from 6 boreholes, (67-22, 45-22, 65-22, 35-23, 75-22, 86-22), and 627 spot measurements were taken on cuttings samples from 2 wells (45A-22, 84B-22).

4. RESULTS

4.1 Spectra Observed

Two smectite minerals were observed at the Fallon FORGE EGS site: montmorillonite and saponite (Figure 4). Smectite minerals are distinguished by large asymmetric absorption features at 1400 nm (related to the O-H bond) and 1900 nm (related to H_2O in the crystal lattice), as well as a smaller feature at ~2200 nm for montmorillonite (related to Al-OH bond), or a feature at ~2300 nm for Saponite (related to Fe-OH bond) (Clark et al., 1990; Clark, 1999). At the Tungsten Mountain geothermal field, montmorillonite was the most common smectite mineral observed (Figure 5).

Both illite and muscovite were identified at Fallon and Tungsten Mountain (Figure 4, 5). Illite/muscovite are distinguished from smectite by narrower absorption features, larger 2200 nm (Al-OH) features relative to 1900 nm features (H_2O), and an additional absorption features at ~2350 nm (Clark et al., 1990; Clark, 1999). Illite is difficult to distinguish from muscovite in the SWIR especially with mixed spectra. However, muscovite tend to have narrower absorption features, and a much smaller 1900 nm feature, which was the criteria for separating those in the present study. Based on the 2200 nm feature, most of the illite/mica observed is of potassic/muscovitic composition. However, at Fallon, there are some intervals where the illite/mica appears to be more phengitic/Fe rich in composition, and at Tungsten Mountain 2200 nm features are suggesting more paragonitic compositions.

Chlorite is a common mineral observed at both Fallon and Tungsten Mountain (Figure 4, 5). Chlorite is distinguished by features at 2250 nm and 2350 nm, related to the Fe-OH and Mg-OH bonds respectively, as well as a 1400 nm features, and a boxy absorption feature at around 1900 nm (Clark et al., 1990). Depending on the composition of the chlorite (more Mg or Fe rich), the strength and

location of these features vary (Clark, 1999). Based on the location of the 2250 nm absorption feature from Fallon and Tungsten, all three chlorite compositions are represented (Mg, Fe-Mg, Fe), although Fe-Mg chlorite was the most common composition at both locations. Most spectra observed interpreted as containing chlorite were mixed with clays and/or carbonates, making accurate identification difficult, especially distinguishing it from other Fe-OH or Mg-OH bearing minerals. However, a few examples of more pure chlorite spectra were observed in close proximity to these mixed spectra. Therefore, chlorite was interpreted to be the cause, although there is a chance that epidote, amphiboles, or other Fe and Mg bearing silicates may also contribute, which have some similar absorption feature locations as chlorite. Further evidence of chlorite is observed in the LWIR from Fallon (Figure 4B).

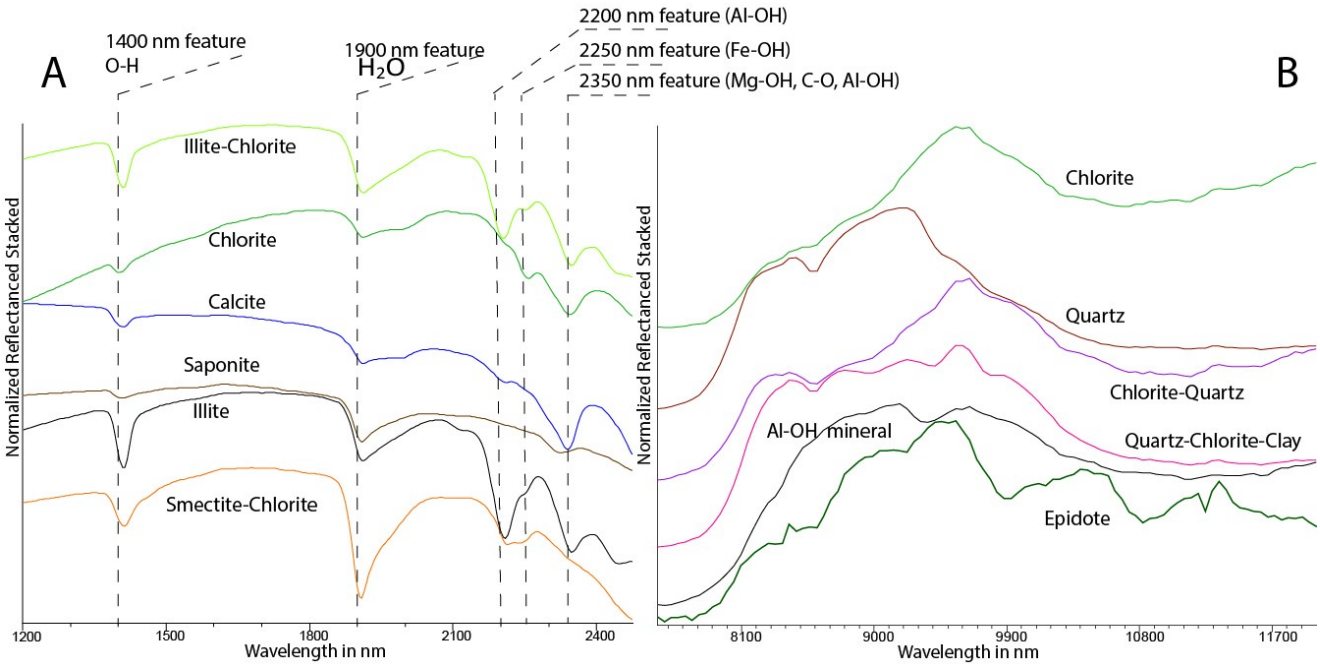

Figure 4: Composite "spectral endmember" spectra observed in cuttings at the Fallon FORGE EGS site well 21-31. (A) Spectra from the SWIR range, with interpretation. (B) Dominant spectra observed in the LWIR wavelength range from the Fallon FORGE site well 21-31 (Kraal and Ayling, 2019).

Calcite was the most common carbonate mineral observed at both locations. However, there may be additional carbonate species at both sites that were not distinguishable due to interference of chlorite and other Fe and Mg bearing minerals that have overlapping absorption features (Figure 4, 5). Carbonates were identified based on a large absorption feature from 2300-2350 nm related to the C-O bond, and a smaller boxy absorption feature near 1900 nm, as well as a few weaker absorption features at 2120, 2000 nm, and 1860 nm (Clark, 1990).

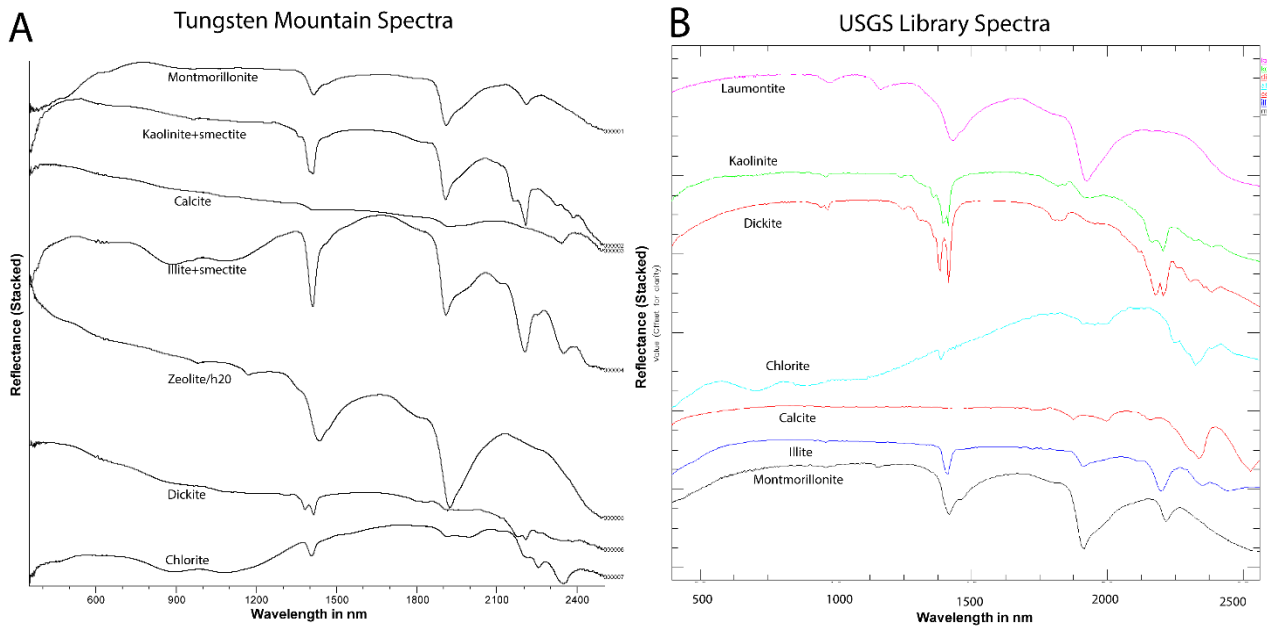

Figure 5: A: Example spectra observed representing mineral endmembers from Tungsten Mountain geothermal field, and interpretation. B: USGS Library Spectra for comparison (Clark et al., 1990).

Kaolinite was observed at Tungsten Mountain and Fallon, and Dickite was observed at Tungsten Mountain (Figure 5). Kaolinite is characterised by an absorption doublet at 1400 + 1416 nm and 2162 + 2208 nm (Clark, 1990; Hauff, 2000). Dickite is also distinguished by two doublets, the first at 1384 + 1414 nm, and 2186 + 2206 nm (Hauff, 2000).

Zeolites were observed at the Tungsten Mountain site (Figure 5). Zeolites are characterised by large, pointy, asymmetric absorption features at 1400 nm and 1900 nm (Clark, 1990). Although some zeolites have additional characteristic features, most zeolites lack distinguishable features from each other, and therefore SWIR is typically not effective for distinguishing between them. Further complications arise because the location of the features is similar to those caused by fluid inclusions containing water, especially in quartz or other silica species. However, absorption features due to fluid inclusions tend to have rounder troughs, which make them distinguishable from the sharper absorption features observed in zeolites.

Quartz was observed in the LWIR at Fallon FORGE (Figure 4). Quartz is distinguished by an absorption doublet between 8000 and 10,000 nm caused by Si-O-Si stretching vibrations (Salisbury et al., 1991). It was also observed as a mixed-spectra, displaying features related to chlorite and aluminium bearing clay minerals (Figure 4).

4.2 Hyperspectral Images from Tungsten Mountain Geothermal System

This study imaged 53 core boxes, from six boreholes ranging in depth from 50 to 1000 meters containing quaternary alluvium sediment. The most common clays observed were overwhelmingly montmorillonite, with illite, chlorite, and kaolinite present but less common (Figure 6). Much of the fine material that makes up the matrix of the alluvium core show montmorillonite, or montmorillonite mixed with illite, chlorite, and/or other smectite clays as the dominant SWIR minerals. In addition, much of the variability in SWIR responsive minerals are confined to large clasts, which sometimes contain illite, chlorite, or calcite spectra. However, there are a few examples where kaolinite clays appear to make up part of the sedimentary matrix.

There are two main units of Tertiary volcanic rocks observed in wells at Tungsten Mountain. The older is Tertiary andesite, (Ta) primarily consisting of andesite, dacite, and volcanoclastics. The youngest is a sequence of felsic ash-flow tuffs (referred to as Tt). The dominant minerals observed in the SWIR in the tuff units are montmorillonite, and kaolinite (Figure 7; Figure 9A). Overall, montmorillonite is more common, and there are alternating zones of montmorillonite rich and kaolinite rich core (see Figure 11 for borehole scale changes). The Tertiary andesite unit was only intersected by a few core wells but displayed mixed spectra of illite, montmorillonite, and chlorite (Figure 9B).

The Triassic meta-sedimentary siltstone/slate unit was intercepted by one core well, 67-22 at depths from 1024 to 1214 meters. In general, this unit consists of dark, spectrally unresponsive siltstone and slate with discreet intervals of more spectrally responsive lighter coloured meta-sedimentary rock, which typically shows clay or chlorite spectral features. This unit is intensely fractured and contains numerous high albedo quartz, calcite, and clay veins (Figure 8). Minerals observed in the SWIR include montmorillonite, illite, chlorite, calcite, and zeolite (Figure 8). Much of the calcite and zeolite are confined to high albedo vein material, commonly along with clay and chlorite spectra.

4.3 Geothermal Well-scale Changes in Mineralogy

The progression of minerals observed at Fallon is from smectite with chlorite (montmorillonite and saponite) to illite ± muscovite with chlorite ± epidote ± carbonate (Figure 6, Figure 10). Between wells, cuttings from well FOH-3D are more chlorite rich than well 21-31 and well 82-36, and this may be due to more andesite layers (Figure 10).

In general, most wells at Tungsten Mountain show a general trend from montmorillonite ± kaolinite, to montmorillonite + illite ± chlorite, to illite + chlorite ± muscovite (Figure 11). This change from smectites to illite/muscovite is observable within the mineral occurrence plots, and the "Illite Maturity" spectral scalar, where overall values tend to increase, meaning stronger Al-OH features relative to H_2O features. Similarly, the 2200 nm wavelength feature tend to be closer to 2208 nm at shallow depths (the location of montmorillonite's Al-OH absorption feature, Clark et al., 1990), and gradually decreases in wavelength with depth, representing a more aluminous muscovitic illite or muscovite composition near 2200 nm. One exception is displayed in well 45A-22, where at 1160 meters there is a sudden change from illite spectra back to montmorillonite, however, as noted in the mudlog this was an interval where "slough" from the overlying crystal tuff unit mixed with the deeper lithologies.

5. DISCUSSION

5.1 Alteration Interpretation

The Fallon FORGE site shows a general trend from low-temperature alteration minerals (such as smectites like montmorillonite and saponite) to higher temperature alteration minerals (such as illite, chlorite, and epidote). This pattern of alteration is similar to those observed in many high-temperature geothermal systems (Henley and Ellis, 1983). However, temperatures at Fallon FORGE are relatively low (less than 214 °C, the highest downhole temperature measured at 2883 m in well 82-36), and permeability is interpreted as low. Therefore, the alteration minerals observed do not match the current thermal/hydrologic conditions, which would suggest smectite minerals rather than epidote, which is typically found in geothermal systems with temperatures higher than 250 °C (Henley and Ellis, 1983). Therefore, our analysis conforms with previous alteration studies of the Fallon area (Jones and Moore, 2013; Kraal and Ayling, 2019) that the high-temperature alteration minerals observed are likely relict from a past higher temperature geothermal system that is no longer active, and the smectite observed represents the current thermal regime. Our analyses add to past interpretations because first, we were able to distinguish between saponite and montmorillonite smectite, and second, we were able to provide higher borehole spatial resolution to delineate alteration mineral assemblage boundaries.

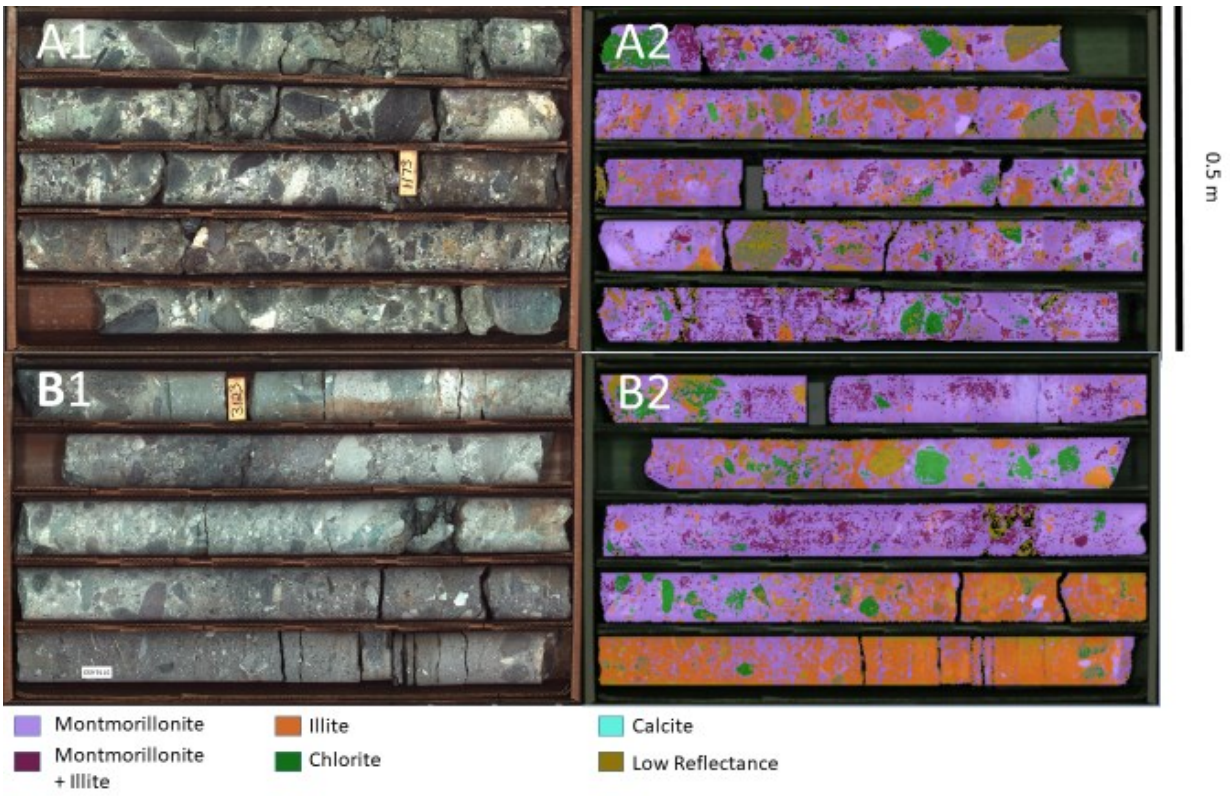

Figure 6: Example core image and SWIR dominant mineral map from Quaternary alluvium at the Tungsten Mountain geothermal field. A1 and A2 are from borehole 67-22 depths 356.6-359.2 m (1170-1178.6 ft), and B1 and B2 are from borehole 67-22 depths 949.4-952.3 m (3114.9-3124.2). The most common mineral in both boreholes is montmorillonite. Much of the chlorite is confined to specific clasts, therefore interpreted as not related to current hydrothermal alteration. In general, illite becomes more common as a SWIR dominant mineral with depth.

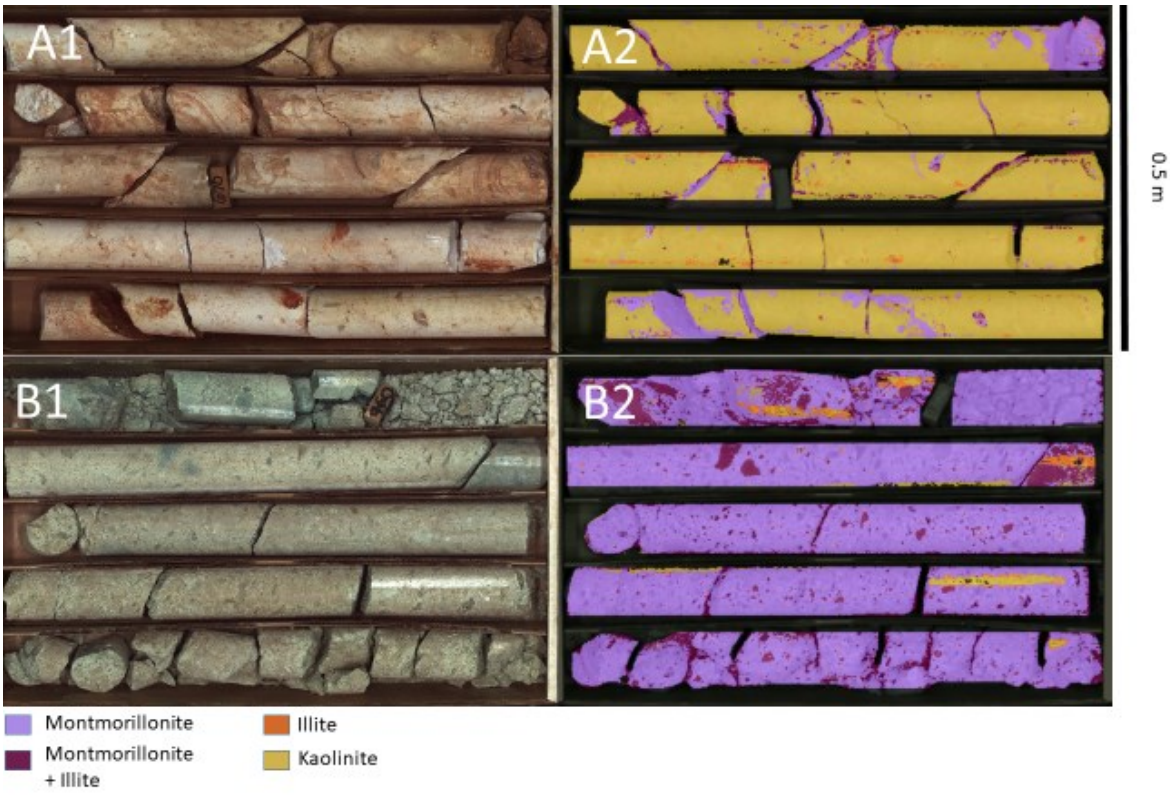

Figure 7: Examples core images and SWIR dominant mineral maps from the Tertiary volcanic units from Tungsten Mountain geothermal field. A1 and A2 show depths 202.2-205.7 m (663.5-675 ft) from the felsic tuff unit. Notice the abundant kaolinite spectra observed as the dominant mineral, with montmorillonite coating fracture faces and veins. B2 and B2 show another box from a member of the Tertiary tuff unit, depths 289.6-292.6 m (950-960 ft) from the same well.

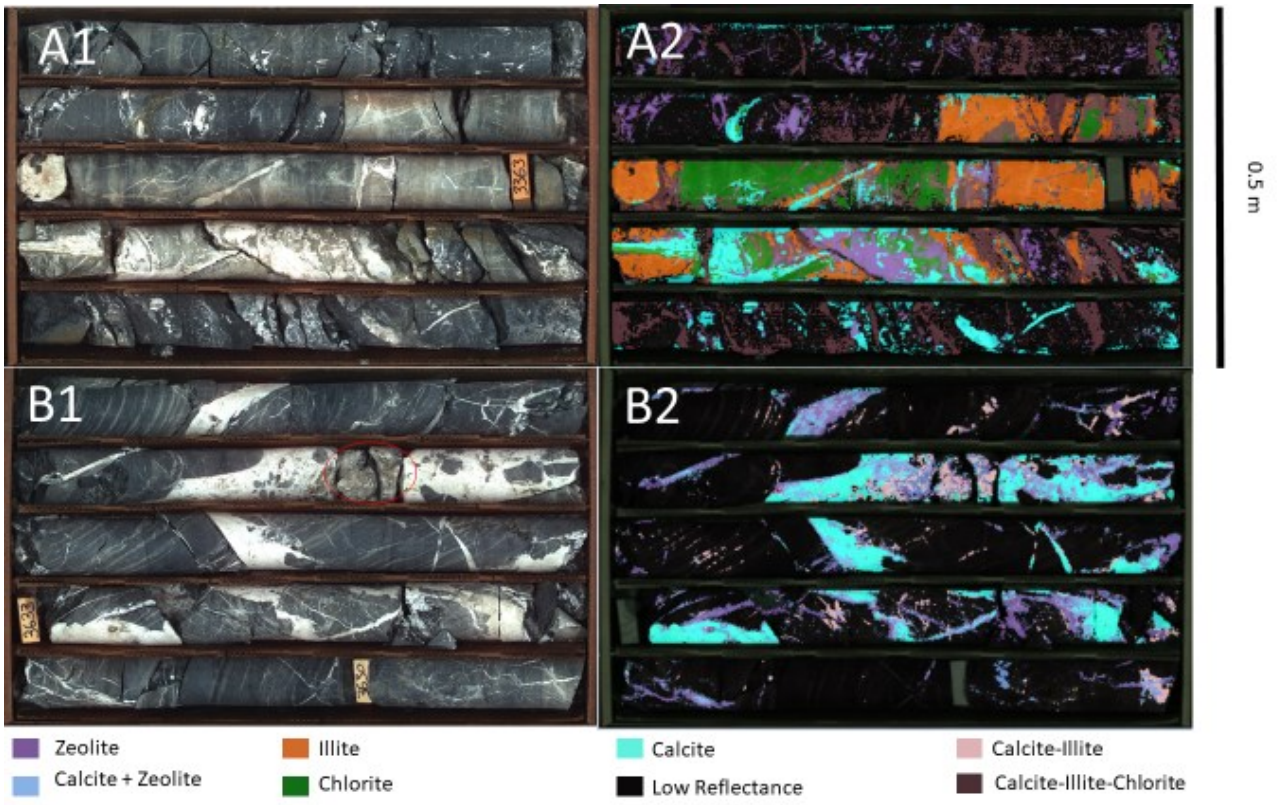

Figure 8: Example core boxes and dominant mineral maps from the Triassic meta-siltstone/slate unit from Tungsten Mountain geothermal field. Both core boxes were taken from BH 67-22, from depths of 1024-1027 m (3358-3368 ft) and 1106-1109 meters (3629-3638 feet) respectively. B1 includes lathe textured calcite in a vein (circled) suggesting boiling at the time of precipitation.

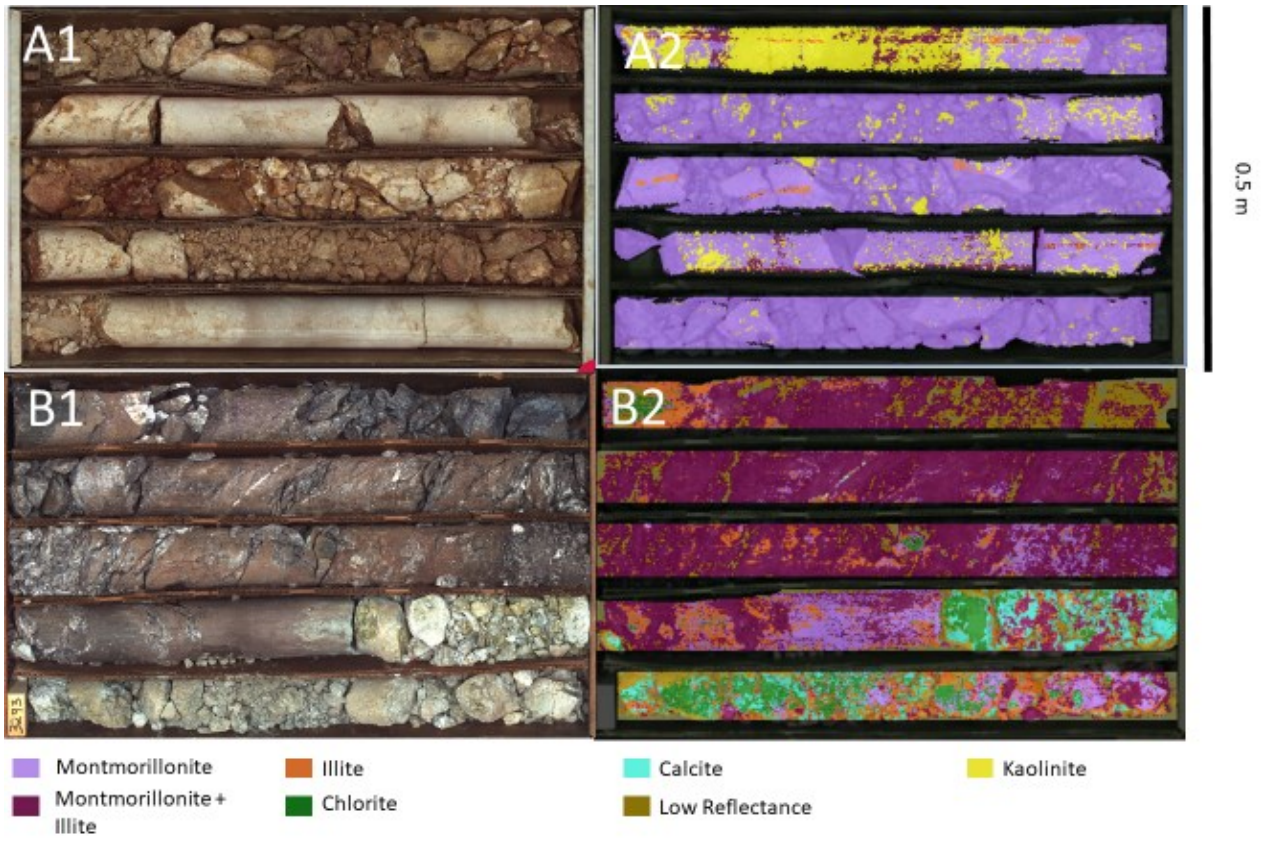

Figure 9: Examples of additional core boxes from Tungsten Mountain geothermal field. Box A is from borehole 65-22 from depths 204-207 m (670-680 ft). Box B is from BH 67-22 depths 1000.7-1004.3 m (3283-3295 ft). Both of these core boxes show fractured material, possibly related to faulting, within the Tertiary tuff unit (A1 and A2), and the Tertiary andesite unit (B1 and B2).

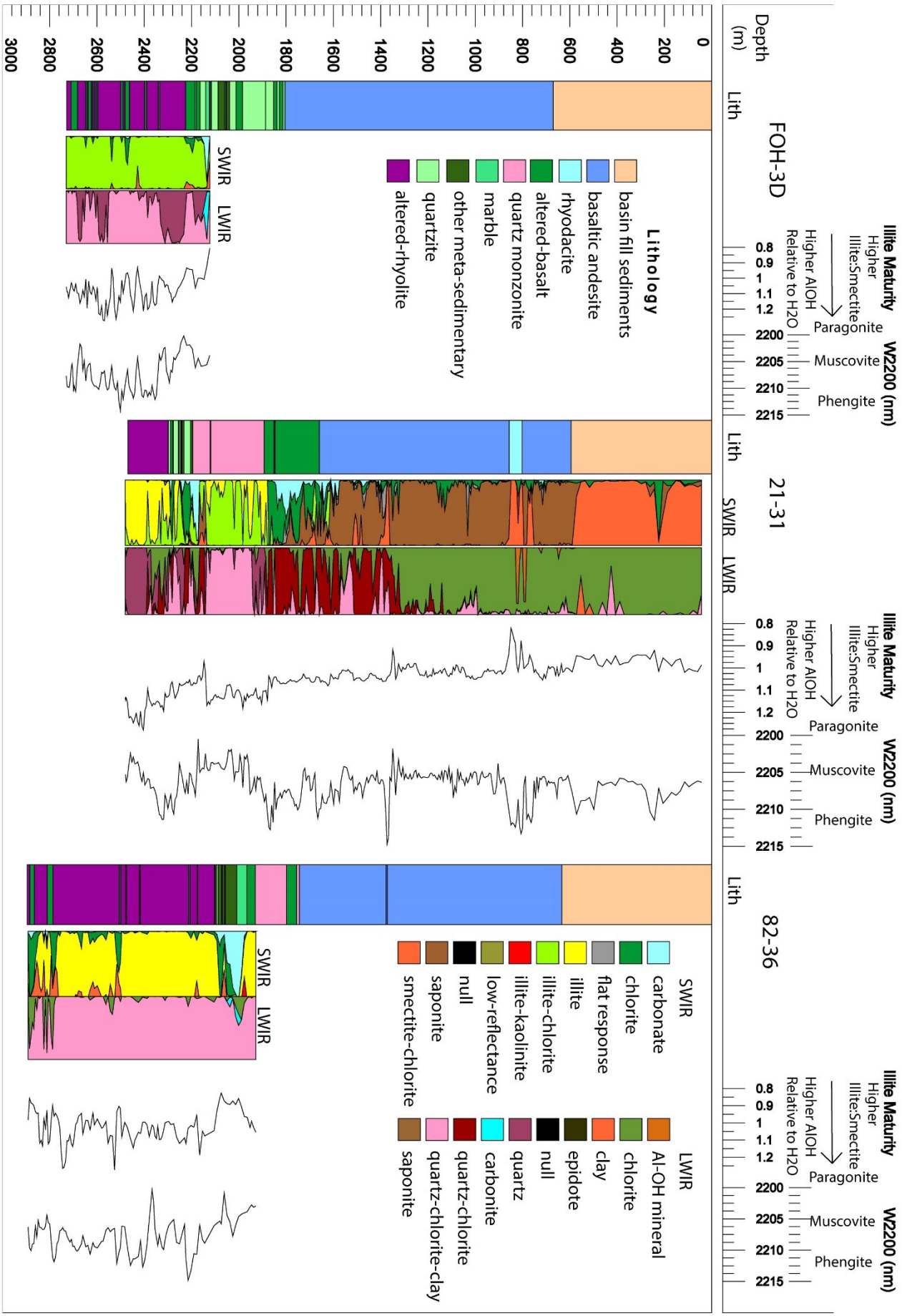

Figure 10: Hyperspectral data summaries from wells 21-31, 82-36, and FOH-3D on the Fallon FORGE site, including spectral scalars "Illite Maturity" and "Wavelength of 2200 nm feature".

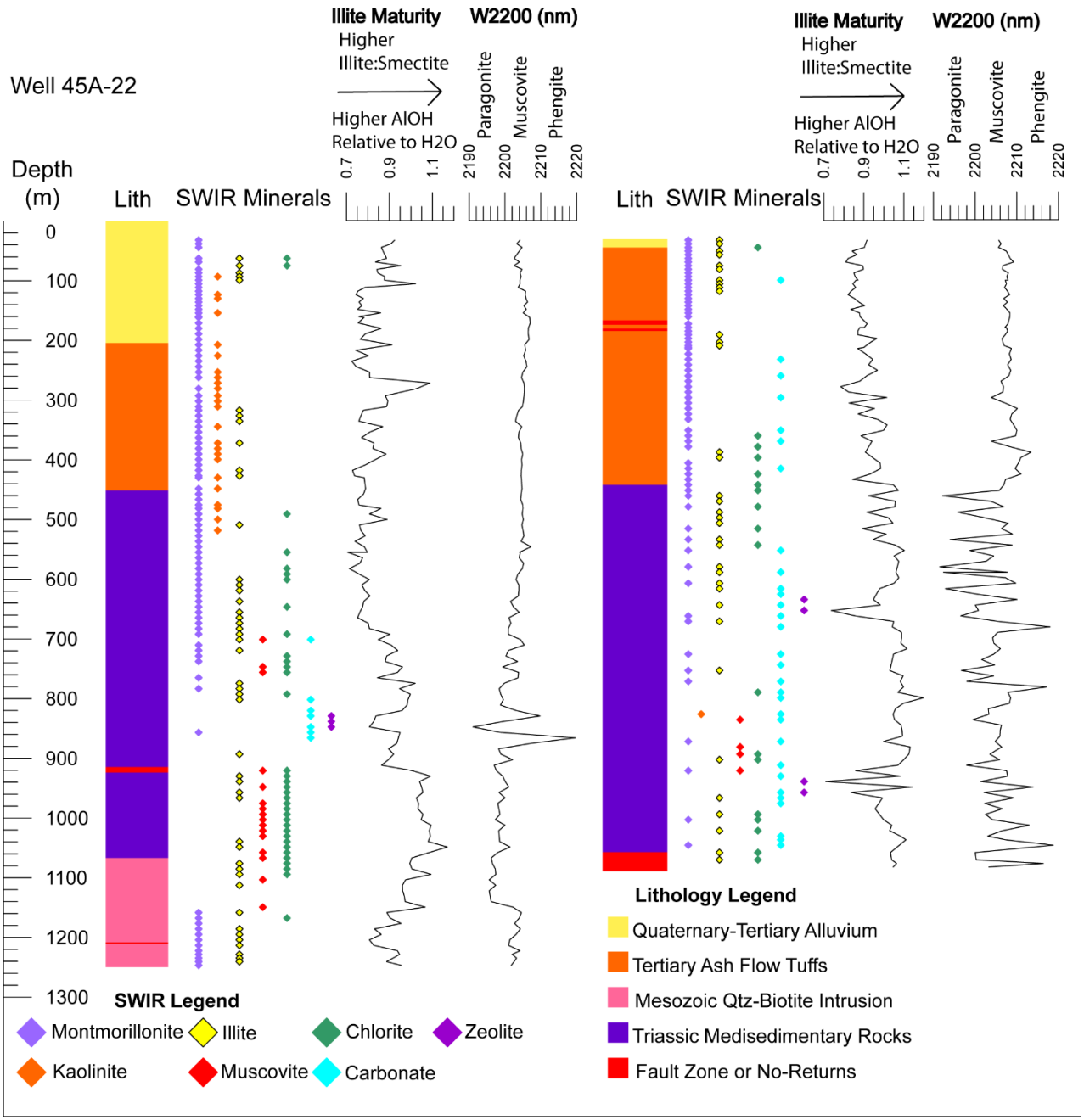

Figure 11: Hyperspectral data from two Tungsten Mountain wells (45A-22, 84B-22) from SWIR point measurements. The plot shows lithology, SWIR mineral identification, and spectral scalars related to mineral chemistry (see text for details).

At Tungsten Mountain, montmorillonite was common throughout most of the core and cuttings samples analysed but was most common within the Quaternary alluvium and Tertiary volcanic units. Kaolinite rich zones within the Tertiary tuff unit were observed in two of the cuttings wells (75B-22, 45A-22), perhaps representing alteration from steam-heated acidic waters on the periphery of the geothermal system, as described over many high-temperature geothermal systems, but may also be a product of weathering (Simmons et al., 2005). Illite and chlorite minerals occurred at shallow depth confined to clasts within the alluvium that are likely relict within the clasts and not due to hydrothermal activity at the current location. Illite and chlorite are interpreted to be products of hydrothermal alteration and occur in the Tertiary volcanic rocks (particularly the Tertiary andesite unit) but are most abundant in the Mesozoic basement section. Muscovite is confined exclusively to the Mesozoic rocks. Dickite and epidote were only observed in a few samples, all within the Mesozoic rocks. The high temperatures suggested by these alteration minerals (>225 °C for illite + chlorite; Henley and Ellis, 1983; Reyes, 1990) were not observed in the wells analysed, which have bottom hole temperatures <150 °C. The coexistence of high temperature minerals with those that are consistent with the current geothermal system may represent the collapse of a previously higher temperature system, or an overprint of an older hydrothermal system, perhaps related to earlier Cenozoic volcanic activity, or as old as the Mesozoic intrusive phase represented by the intrusive rocks observed at the site. Based on this evidence of multiple possible hydrothermal systems, this site may be particularly favourable for hydrothermal activity, perhaps

due to tectonic favourability, and/or deeper crustal pathways, but further analyses are required to confirm these speculations. Analysis of the current fluid's chemical equilibrium with the mineral assemblages observed could also further provide insight, such as the degree of disequilibrium.

Previous XRD and petrographic studies for analogous low-temperature alteration in geothermal fields have found minerals useful for distinguishing between fossil fluid flow pathways (for example illite representing earlier stages of hydrothermal alteration), and current fluid flow locations (kaolinite rich intervals) (Mas et al., 2003). At Tungsten Mountain, no obvious spectral variables have yet been found to distinguish between current and past hydrothermal alteration. However, additional petrographic, XRD and Scanning Electron Microscope (SEM) studies of selected intervals may provide new insight to aid in the interpretation of the hyperspectral data. The fact that both locations (Fallon and Tungsten) show similar patterns of increasing alteration grade provides an example of the difficulties in applying alteration studies to low-temperature geothermal systems that overprint possible earlier phases of hydrothermal activity, common in the Great Basin region of the western USA. Difficulties in interpretation of hyperspectral data suggest additional petrographic work is required to understand the paragenesis of various alteration minerals observed. Despite these limitations, infrared spectroscopy has been shown to be a valuable tool for rapidly identifying the distribution of clay minerals with high spatial resolution, at multiple scales (e.g. core box, borehole, between wells).

5.2 Applications of Hyperspectral Core Images

Hyperspectral core images allowed for additional interpretive ability, particularly in terms of spatial relationships of minerals. Two observations were especially relevant for the present analysis. Imaging of the Quaternary alluvium intervals at Tungsten Mountain showed more spectral variability within clasts. This observation is useful for interpreting spectra from cuttings samples: since many of the shallow alluvium cuttings samples showed spectra suggesting illite, chlorite, and muscovite, these are likely due to their existence in the parent rock of the sedimentary clasts. However, with depth, these "higher temperature" minerals became less common within the alluvial sediments, perhaps suggesting well intervals where hydrothermal alteration has reset the clays to something closer to the current thermal regime. In addition, hyperspectral images can be useful to distinguish between a vein or fracture-related alteration minerals, and host rock alteration. For example: for some intervals, kaolinite was the dominant SWIR responsive mineral in the wall-rock, but montmorillonite associated with red clay that coats fracture faces and veins, possibly associated with the current hydrothermal activity (Figure 8A). Similarly, in the Triassic slate units, extensive calcite, chlorite, illite, and zeolite veining were observed, in contrast to low reflectance metasedimentary host rock (Figure 9). Therefore, hyperspectral images can be used to distinguish clay mineralogy derived from wall-rock, vein material, and sedimentary clasts, which would be difficult with traditional methods, allowing for new interpretive opportunities.

6. CONCLUSION

Overall, this study shows that hyperspectral imaging can provide useful information about the spatial distribution of spectrally responsive hydrothermal alteration minerals found in geothermal systems. Zonation of hydrothermal alteration minerals was found with depth, and between wells at both Fallon FORGE and Tungsten Mountain geothermal field. However, the mismatch between current thermal/hydrologic conditions, and observed hydrothermal alteration minerals suggest that care must be taken for interpretation of thermal regime from hydrothermal alteration minerals found in geothermal systems in the Great Basin region of the western United States due to the long history of regional hydrothermal alteration, and the likelihood of hydrothermal systems occurring at the same location as fossil hydrothermal systems under different geochemical and thermal conditions. In addition, this study suggests the importance of petrography for interpreting the hydrothermal alteration minerals found within geothermal systems. The capabilities of hyperspectral core imaging allow for analysis of spatial relationships of minerals at different scales than possible with petrography and XRD alone, allowing for a new analysis of the zonation of hydrothermal alteration minerals. Future work proposed includes more detailed petrography of samples, additional hyperspectral imaging to create a more continuous dataset, and SEM to investigate the possible overprinting of high-temperature clays by low-temperature clays to confirm the hypothesis inspired by the current hyperspectral interpretation.

ACKNOWLEDGEMENTS

New data acquisition in the Fallon FORGE well 21-31 was funded by US Department of Energy grant EE0007160 awarded to Sandia National Laboratories, with a subcontract to the University of Nevada, Reno. We would like to thank the entire Fallon FORGE team. We also thank Ben Delwiche and Ormat Nevada, Inc. for access to their core, cuttings, and data regarding the Tungsten Mountain geothermal field. We also thank the TerraCore team for aid in acquiring hyperspectral image data, including Dave Browning, Paul Linton, Jared Landers, Kyle Landers, and Brandon Rasmussen. Lastly, we would like to acknowledge UNR student Bryce Ford for aid in moving heavy core boxes.

REFERENCES

Ayling, B.: Geothermal Energy, from Muntean, J.L., Davis, D.A., and Ayling, B.: The Nevada Mineral Industry 2017 [online version]: Nevada Bureau of Mines and Geology Special Publication MI-2017 (2018). p. 168-187

Ayling, B., Huntington, J., Smith, B., Edwards, D.: Hyperspectral logging of middle Cambrian marine sediments with hydrocarbon prospectivity: a case study from the southern Georgina Basin, northern Australia, *Australian Journal of Earth Sciences*, v. 63(8), (2016). p. 1069–1085.

Blankenship, Doug, Hinz, Nicholas, and Faulds, James: Fallon, Nevada FORGE Lithology Logs and Well 21-31 Drilling Data. United States: N. p., (2018). Web. doi:10.15121/1452754.

Browne, P. R. L.: Hydrothermal alteration in active geothermal fields, *Annual review of earth and planetary sciences*, 6(1), (1978). 229-248.

Burke, D.B., and Silberling, N.J.: The Auld Lang Syne Group of Late Triassic and Jurassic (?) age, north-central Nevada: Contributions to Stratigraphy*, U.S, Geological Survey Bulletin* 1394-E, (1973). 14 p.

Calvin, W.M. and E. L. Pace: Alteration in geothermal drill core using a field-portable spectroradiometer, *Geothermics*, Vol. 61, (2016). 12-23.

Clark, R.N.: Spectroscopy of rocks and minerals, and principles of spectroscopy, Manual of remote sensing 3, no. 3-58 (1999). 2-2.

Clark, R. N., King, T.V., Klejwa, M., Swayze, G.A., and Vergo, N.: High spectral resolution reflectance spectroscopy of minerals. *Journal of Geophysical Research*: Solid Earth 95, no. B8 (1990). 12653-12680.

DeCelles, P. G.: Late Jurassic to Eocene evolution of the Cordilleran thrust belt and foreland basin system, western USA*, American Journal of Science* 304, no. 2 (2004). 105-168.

Delwiche, B., Peters, B., Sophy, M., Smith, C., and O'Brien, J.: Successful Deployment of a Multi-Crossing Directional Drilling Method at Ormat's New Tungsten Mountain Geothermal Field in Churchill County, Nevada*, PROCEEDINGS*, 43rd Workshop on Geothermal Reservoir Engineering, Stanford University, Stanford, Ca, February 12-14, (2018). SGP-TR-213

Dezayes, C., Genter, A., Valley, B.: Structure of the low permeable naturally fractured geothermal reservoir at Soultz. *Comptes Rendus Géoscience, Elsevier Masson*, 343 (7-8), (2003), 517-530. ff10.1016/j.crte.2009.10.002ff. ffhal-00492278f

Dickinson, W.R.: Evolution of the North American cordillera, *Annu. Rev. Earth Planet. Sci*. 32, (2004), 13-45.

Dickinson, W.R.: Geotectonic evolution of the Great Basin, *Geosphere* 2, no. 7, (2006), 353-368.

Faulds, J.E., Coolbaugh, M., Blewitt, G., and Henry, C.D: Why is Nevada in hot water? Structural controls and tectonic model of geothermal systems in the northwestern Great Basin*: Geothermal Resources Council Transactions*, v. 28, (2004), 649-654.

Faulds, J.E., Henry, C.D., and Hinz, N.H.: Kinematics of the northern Walker Lane: An incipient transform fault along the Pacific–North American plate boundary, *Geology* 33, no. 6, (2005), 505-508.

Faulds, J.E., Hinz, N.H., Siler, D. L., Glen, J.M.G., Fortuna, M.A., Queen, J.H., Blake, K., Fallon FORGE Team: Update on the Stratigraphic and Structural Framework of the Proposed Fallon FORGE site, Nevada, *GRC Transactions*, Vol. 42, (2018).

Frolova, J., Ladygin, V., Rychagov, S., and Zukhubaya, D.: Effects of hydrothermal alterations on physical and mechanical properties of rocks in the Kuril–Kamchatka island arc*, Engineering Geology*, 183, (2014), 80-95.

Geiger, C.A.: An introduction to spectroscopic methods in the mineral sciences and geochemistry. Ch. 1 in EMU Notes in Mineralogy, Vol.6, A.Beran and E. Libowitzky, Eds, (2004).

Glaas, C., Vidal, J., Patrier, P., Girard, J. F., Beaufort, D., Petit, S., & Genter, A. (2019). How Do Secondary Minerals in Granite Help Distinguish Paleo-from Present-Day Permeable Fracture Zones? Joint Interpretation of SWIR Spectroscopy and Geophysical Logs in the Geothermal Wells of Northern Alsace. *Geofluids*, *2019*.

Hauff, P. L.: Applied Reflectance Spectroscopy with emphasis on Data Collection and Data Interpretation using the PIMA-II Spectrometer. Spectral International, Inc., May 1993, (2000).

Henley, R.W., Brown, K.L.: A practical guide to the thermodynamics of geothermal fluids and hydrothermal ore deposits, in Berger, B.R., Bethke, P.M., ed., Geology and geochemistry of epithermal systems, *Reviews of Economic Geology*, v. 2, (1985), 25–43.

Henley, R. W., & Ellis, A. J.: Geothermal systems ancient and modern: a geochemical review, *Earth-science reviews*, 19(1), (1983) 1-50.

Henry, C. D., Hinz, N.H., Faulds, J., Colgan, J.P., John, D.A., Brooks, E.R., Cassel, E.J., Garside, L.J., Davis, D.A., and Castor, S.B.: Eocene–Early Miocene paleotopography of the Sierra Nevada–Great Basin–Nevadaplano based on widespread ash-flow tuffs and paleovalleys*, Geosphere* 8, no. 1, (2012), 1-27.

Henry, C.D., and John, D.A.: Magmatism, ash-flow tuffs, and calderas of the ignimbrite flare-up in the western Nevada volcanic field, Great Basin, USA: *Geosphere,* v. 9, (2013), 951–1008, doi: 10.1130 /GES00867.1.

Herrmann, W., Blake, M., Doyle, M., Huston, D., Kamprad, J., Merry, N., and Pontual, S.: Short wavelength infrared (SWIR) spectral analysis of hydrothermal alteration zones associated with base metal sulfide deposits at Rosebery and Western Tharsis, Tasmania, and Highway-Reward, Queensland, *Economic Geology* 96, no. 5, (2001), 939-955.

Huntington, J. F., Mauger, A. J., Skirrow, R. G., Bastrakov, E. N., Connor, P., Mason, P., ... & Whitbourn, L. B.: Automated mineralogical core logging at the Emmie Bluff iron oxide-copper-gold prospect, *MESA Journal*, 41, (2006), 38-44.

John, D.A., du Bray, E.A., Henry, C.D. and Vikre, P.G.: Cenozoic magmatism and epithermal gold-silver deposits of the southern Ancestral Cascade Arc, Western Nevada and Eastern California*: Geological Society of Nevada,* (2015).

Jones, C.G., and Moore, J.N.: Petrographic and X-ray Diffraction Study of 4 Wells from Naval Air Station Fallon, Churchill County, Nevada: Report for the Navy Geothermal Program Office, (2013), Contract Number N62473_13_M_1404.

Kokaly, R. F., Graham, G. E., Hoefen, T. M., Kelley, K. D., Johnson, M. R., Hubbard, B. E., ... & Prakash: A. Multiscale Hyperspectral Imaging of the Orange Hill Porphyry Copper Deposit, Alaska, USA, with Laboratory-, Field-, and Aircraft-based Imaging Spectrometers. Conference Paper October 2017, *Spectral Geology and Remote Sensing*, Paper 84, (2017).

Kraal, K. O., Ayling, B., Calvin, W., & Browning, D.: Comparison of a Portable Field Spectrometer and Automated Imaging on Geothermal Drill Core: A Pilot Study. *GRC Transactions* Vol. 42, (2018), 1327-1339.

Kraal, K. O., & Ayling, B.: Hyperspectral Characterization of Fallon FORGE Well 21-31: New Data and Technology Applications, *PROCEEDINGS*, 44th Workshop on Geothermal Reservoir Engineering, Stanford University, Stanford, California, February 11-13, (2019), SGP-TR-214.

Kraal, K. O., Ayling, B. F., Blake, K., Hackett, L., Perdana, T. S. P., & Stacey, R. (2021). Linkages between hydrothermal alteration, natural fractures, and permeability: Integration of borehole data for reservoir characterization at the Fallon FORGE EGS site, Nevada, USA. *Geothermics*, *89*, 101946.

Machette, M.N., Haller, K.M., Okumura, K., Ruleman, C.A., Debray, S., and Mahan, S.: Paleoseismology of the Clan Alpine fault, west-central Nevada, *Geological Society of America Abstracts with Program*, (2002), https://gsa.confex.com/gsa/2002RM/finalprogram/abstract_33718.htm.

Machette, M.N., Haller, K.M., Ruleman, C.A., Mahan, S., and Okumura, K.: Geologic evidence for late quaternary movement on the Clan Alpine Fault, west-central Nevada : Trench logs, scarp profiles, location maps, and sample and soil descriptions: *U.S. Geological Survey Scientific Investigations* Map 2891, 1 sheet, https://pubs.er.usgs.gov/publication/sim2891, (2005).

Mas, A., Patrier, P., Beaufort, D., & Genter, A.: Clay-mineral signatures of fossil and active hydrothermal circulations in the geothermal system of the Lamentin Plain, Martinique. *Journal of volcanology and geothermal research*, 124(3-4), (2003), 195-218.

Mauger, A. J., Keeling J. L., and Huntington, J. F.: Alteration mapping of the Tarcoola Goldfield (South Australia) using a suite of hyperspectral methods, *Applied Earth Science* 116, no. 1, (2007), 2-12.

Mauriohooho, K, Barker, S.L., Rae, A.J., and Simpson, M.P.: Hydrothermal alteration and whole rock geochemistry of the Tauhara geothermal field: traditional versus rapid techniques, In *Proceedings* 36th New Zealand Geothermal Workshop, vol. 24, (2014), 26.

Mehmani, Y., Burnham, A. K., Berg, M. D. V., & Tchelepi, H. A.: Quantification of organic content in shales via near-infrared imaging: Green River Formation. *Fuel*, 208, (2017), 337-352.

Pontual, S., Merry, N. and Gamson, P.: Spectral interpretation field manual, Spectral Analysis Guide for Mineral Exploration 1 (1997).

Reyes, A.G.: Petrology of Philippine geothermal systems and the application of alteration mineralogy to their assessment. *J. Volcanol. Geotherm Res*., 43, (1990), 279-309.

Salisbury, J.W., Walter, L. S., Vergo, N., and D'Aria, D. M.: Infrared (2.1-25 um) spectra of minerals, *John Hopkins University Press.* (1991).

Siler, D. L., Hinz, N. H., Faulds, J. E., Tobin, B., Blake, K., Tiedeman, A., ... & Rhodes, G.: The geologic framework of the Fallon FORGE site. *Geothermal Resources Council Transactions*, 40, (2016), 573-584.

Siler, D. L., Hinz, N. H., Faulds, J. E., Ayling, B., Blake, K., Tiedeman, A., Sabin, A., Blankenship, D., Kennedy, M., Rhodes, G., Sophy, M. J., Glen, J. M.G., Phelps, G. A., Fortuna, M., Queen, J., Witter, J.: The Geologic and Structural Framework of the Fallon FORGE site*, PROCEEDINGS* 43rd Workshop on Geothermal Reservoir Engineering, Stanford University, Feb 12-14, (2018), SGP-TR-213.

Siler, D.L., Faulds, J.E., Glen, J.M.G., Hinz, N.H., Witter, J.B., Blake, K., Queen, J., Fortuna, M., (2019). Three-dimensional geologic map of the sourthern Carson sink, Nevada, including the Fallon FORGE area. U.S. Geological Survey Scientific Investigations Map 3437, p. 22. https://doi.org/10.3133/sim3437 pamphlet.

Simmons, S. F., Browne , P. R. L., Arehart, G. B., and Hulston, J. R.: Illite, illite-smectite and smectite occurrences in the Broadlands-Ohaaki geothermal system and their implications for clay mineral geothermometry. *Water rock interaction*, 9, (1998), 691-694.

Simmons, S.F., White, N.C., and John, D.A.: Geological Characteristics of Epithermal Precious and Base Metal Deposits, Economic Geology 100th Anniversary Volume, (2005), 485-522.

Simpson, M. P., and Rae, A. J.: Short-wave infrared (SWIR) reflectance spectrometric characterization of clays from geothermal systems of the Taupo Volcanic Zone, New Zealand, *Geothermics,* 73, (2018), 74-90.

Thatcher, W., Foulger, G.R., Julian, B. R., Svarc, J., Quilty, E., Bawden, G.W.: Present-Day Deformation Across the Basin and Range Province, Western United States. *Science*, 12 Mar 199, Vol. 283, Issue 5408, (1999), 1714-1718.

Thompson, A. J.: Alteration mapping in exploration: Application of short wave infrared (SWIR) spectroscopy*, Econ. Geol. Newsl.,* 30, (1999), 13.

Van Buer, N.J., Miller, E.L., and Dumitru, T.A., Early Tertiary paleogeologic map of the northern Sierra Nevada batholith and the northwestern Basin and Range*: Geology* v. 37,no. 4, (2009), 371-374.

Waweru, K. M. (2019). *Characterization of hydrothermal minerals in up-flow, out-flow and cold in-flux zones in olkaria geothermal system using SWIR hyperspectral imaging technique* (Master's thesis, University of Twente).

Willden, R., and Speed, R.C.: Geology and Mineral Deposits of Churchill County, Nevada: *Nevada Bureau of Mines and Geology Bulletin* 83, (1974), 92.

Williams, C.F., Reed, M.J., DeAngelo, J., and Galanis, S.P. Jr.: Quantifying the undiscovered geothermal resources of the United States, *GRC Transactions*, v. 33, (2009), 995-1002.

Wyering, L. D., Villeneuve, M. C., Wallis, I. C., Siratovich, P. A., Kennedy, B. M., Gravley, D. M., & Cant, J. L.: Mechanical and physical properties of hydrothermally altered rocks, Taupo Volcanic Zone, New Zealand, *Journal of Volcanology and Geothermal Research*, 288, (2014), 76-93.

Wyld, Sandra J.: Structural evolution of a Mesozoic backarc fold-and-thrust belt in the US Cordillera: New evidence from northern Nevada., *Geological Society of America Bulletin* 114, no. 11, (2002), 1452-1468.

Yang, K., J. F. Huntington, P. R. L. Browne, and C. Ma, An infrared spectral reflectance study of hydrothermal alteration minerals from the Te Mihi sector of the Wairakei geothermal system, New Zealand, *Geothermics*, 29(3), (2000), 377-392.

Yang, K., P. R. L. Browne, J. F. Huntington, and J. L. Walshe, Characterising the hydrothermal alteration of the Broadlands-Ohaaki geothermal system, New Zealand, using short-wave infrared spectroscopy, *Journal of Volcanology and Geothermal Research,* 106(1-2), (2001), 53-65.

Zhou, X., Jara, C., Bardoux, M., & Plasencia, C.: Multi-Scale integrated application of Spectral Geology and Remote Sensing for Mineral Exploration. Conference Paper October, *Spectral Geology and Remote Sensing*, Paper 82, (2017).